



Reactive transport modeling of scale precipitation and deposition during incompatible water injection in carbonate reservoirs

A. Shojaee¹ · S. Kord¹  · R. Miri² · O. Mohammadzadeh³

Received: 13 April 2023 / Accepted: 7 October 2023 / Published online: 25 October 2023
© The Author(s) 2023

Abstract

Seawater injection is an efficient enhanced oil recovery (EOR) method that capitalizes on the chemical composition differences between the injecting seawater and in-situ formation water, which leads to physicochemical interactions between the rock and fluids. These rock and fluid interactions result in changes of rock wettability and subsequent improved microscopic sweep efficiency. However, the ion imbalance resulting from seawater injection and its incompatibility with the in-situ formation water may interfere with the rock and fluids equilibrium state, causing scale precipitation and subsequent deposition which can negatively impact rock quality, well productivity and reservoir performance. In this study, an accurate, robust, and general approach is presented by coupling a geochemical module with a compositional two-phase fluid flow model to handle reactive transport in porous media. The proposed coupled model, so-called ad-scale model, is capable of simulating carbonate rock dissolution and sulfate scale formation/deposition for evaluating reservoir performance under incompatible water injection. The model predictions were validated using experimental data. This model was also utilized to predict water injection rate into a carbonate formation. It was obtained that both the reacting and non-reacting component profiles were accurately predicted using the proposed coupled model. The water injection rate prediction was also validated and showed high accuracy with absolute error and coefficient of determination values of 9.02% and 0.99, respectively. In addition, a sensitivity analysis was performed on water composition, which showed a strong dependence of reservoir and well performance on water composition.

✉ S. Kord
sh.kord@put.ac.ir

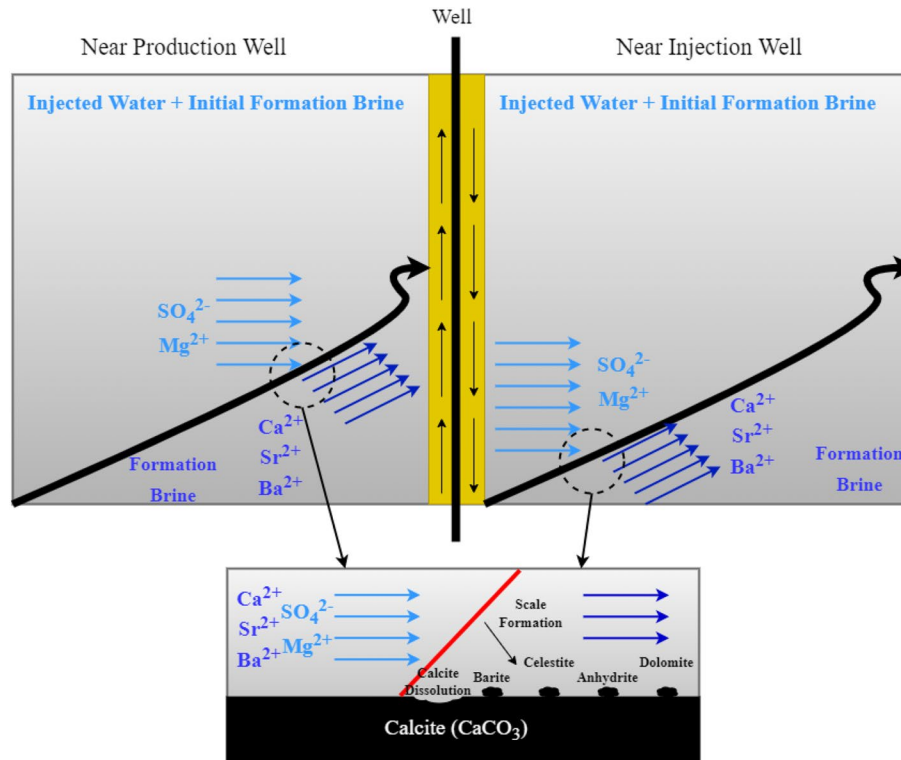
¹ Ahwaz Faculty of Petroleum, Petroleum University of Technology, Ahwaz, Iran

² School of Chemical Engineering, Iran University of Science and Technology (IUST), P.O. Box 16765-163, Tehran, Iran

³ Department of Process Engineering, Memorial University, St. John's, NL, Canada

Graphical abstract

This diagram elucidates what exactly happens during incompatible water injection in the mixing zones near the injection well (right half of the figure) or production well (left half of the figure) where most of the geochemical phenomena occur.



Keywords Reactive transport modelling · Scale formation · Formation damage · Smart water · Well injectivity decline

Abbreviations

FW	Formation water
MRST	MATLAB reservoir simulation toolbox
S.I.	Saturation index
SW	Sea water

List of Symbols

α	Phase (oil, water)
β	Formation damage factor
φ	Porosity ($\frac{m^3}{m^3}$, fraction)
λ	Mobility
μ	Viscosity (Pa.s)
ρ	Density ($\frac{kg}{m^3}$)
$D_{i,\alpha}$	Diffusion coefficient of component i in phase α ($\frac{m^2}{s}$)
g	Gravitational constant ($\frac{m}{s^2}$)
h	Height (m)
i	Component indicator
IAP	Ion activity product
K	Absolute permeability (m^2)
K_{eq}	Solubility product
$k_{r\alpha}$	Relative permeability of phase α

N_c	Number of components
N_p	Number of phases
O	Oil phase
P	Pressure (Pa)
q_i	Flow rate of component i ($\frac{m^3}{s}$)
S_α	Saturation of phase α
T	Transmissibility ($\frac{m^3}{Pa.s}$)
v_α	Velocity of phase α ($\frac{m}{s}$)
V	Volume (m^3)
W	Water phase
$x_{i,\alpha}$	Mass of component i per one kilogram of phase α ($\frac{kg}{kg}$)
z	Depth (m)

Introduction

Waterflooding is an important part of most secondary or tertiary recovery processes during which the injected water, mostly seawater for the case of offshore oilfields, is injected for pressure maintenance, increasing sweep efficiency, and

mobilization of the residual oil when combined with some surface-active agents to change the chemical equilibrium between the rock and fluids. There are some downsides associated with injecting an aqueous phase with dissolved salt content different than that of the in-situ formation brine (Mackay 2003). This chemical incompatibility between the in-situ formation brine and injected aqueous phase could result in inorganic scale precipitation, which could ultimately cause scale deposition in the near wellbore region as well as deep into the reservoir, depending on the flow dynamics and rock and fluid properties (Mackay 2003). This could result in potential permeability impairment, flow diversion, injectivity reduction and loss of oil production which negatively impact the economics of oil production (Bajammal et al. 2013; Bedrikovetsky et al. 2009a, b; Bedrikovetsky et al. 2004; Bedrikovetsky et al. 2009a, b; Haghtalab et al. 2014; Hajirezaie et al. 2017; Hajirezaie et al. 2019; Mackay et al. 2003b; Masoudi et al. 2020; Moghadasi et al. 2006; Parvin et al. 2020; Rocha et al. 2001). Reduction of well injectivity/productivity is a common problem when it comes to incompatible water injection scenarios (Jordan et al. 2008; Mackay et al. 2003a). For instance, a 75%

injectivity reduction over a six-year period was reported by Moghadasi et al. (2004) in an oilfield in Iran due to incompatible water injection. It is therefore imperative to study this phenomenon using experimental and numerical simulation methods.

The major triggering mechanism for inorganic salt precipitation during waterflooding was proved to be disturbing the chemical equilibrium between fluids and rock due to incompatibility between the injecting water and in-situ formation water (Mackay et al. 2003b; Moghadasi et al. 2004; Oddo and Tomson 1994; Rocha et al. 2001; Sorbie and Mackay 2000; Yuan et al. 1994). Various attempts have been made in the literature to develop predictive models for inorganic scale precipitation and deposition. Some of these studies were only focusing on modeling the precipitation and deposition processes, whereas some provided experimental data to validate the proposed models. Some of these studies are briefly listed in Table 1. A more detailed review of several other research articles is also provided in the upcoming paragraphs.

Oddo and Tomson (1994) developed the so-called Saturation Index (S.I.) scale formation model. Based on the

Table 1 Summary of some studies focusing on scale formation, precipitation and deposition

References	Methodology	Results
Yuan et al. (1994)	Static incompatible water mixing	Calculating saturation index
Mackay et al. (2003a, b)	Scaling risk assessment	Predicting well injection considering scale formation
Moghadasi et al. (2006)	Semi-empirical model validated with experiments	Investigated the effect of pressure, temperature, and pH on scaling tendency
P. Bedrikovetsky et al. (2009a, b)	Prediction of sulfate precipitation based on well data	Measuring sulfate scaling parameter using well data
Amiri et al. (2012)	OLI Scale Chem software	Investigating the effect of pressure and temperature on scaling tendency
Shirdel (2013)	Coupling UTCHEM with PHREEQC	Predicting asphaltene deposition in the near-wellbore region
Safari and Jamialahmadi (2014)	Thermodynamic, kinetic, and fluid flow in porous media model	Predicting single salt (i.e., barium sulfate) precipitation
Huber et al. (2014)	Pore-scale model for the advection–diffusion reactive flow in porous media using lattice Boltzmann theory	Predicting permeability and porosity changes during dissolution and precipitation processes
Haghtalab et al. (2014)	Thermodynamics of scale formation due to incompatible water injection	Optimizing the adjustable parameters of ENRTL model for sulfate scales
Abouie (2015)	Coupling UTWELL with IPHREEQC	Modeling scale precipitation along the wellbore
Hajirezaie et al. (2017)	Empirical model based on experimental data	Determining permeability and porosity reduction during incompatible water injection
Ozen (2017)	Coupling UTCHEM with kinetic reactions	Investigating the effect of scale precipitation during ASP flooding
Hu and Mackay (2018)	1-D reactive model based on filed data	Predicting calcite dissolution and anhydrite precipitation during seawater injection
Hajirezaie et al. (2019)	Simulation using CMG-GEM and ScaleSoftPiterz	Investigating the effect of scale formation on recovery factor
Shabani et al. (2019a, b)	Coupling PHREEQC with fluid flow in porous media model	Simulating scale formation during incompatible waterflooding
Mahmoodi and Nick (2022)	Coupling a commercial reservoir simulator with a component transport model and a chemical model	Investigating the interplay between reservoir souring and barite formation due to seawater injection

definition and value of the S.I., it is determined whether the aqueous phase could dissolve more salt or not. The S.I., defined as a function of ion activity and salt solubility, represent an undersaturated, saturated, and supersaturated state when $S.I. < 0$, $S.I. = 0$, and $S.I. > 0$, respectively. In the case of sulfate salts, supersaturation occurs in low concentration of calcium, strontium, and barium in the presence of sulfate ions. There are some experimental studies that focus on permeability impairment due to inorganic scale precipitation and deposition (Abbasi et al. 2020; Merdhah et al. 2008; Zohoorian et al. 2016). For instance, Todd and Yuan (1992) conducted an experimental study on barium sulfate scaling and concluded that minor reductions in porosity could lead to significant permeability impairment due to scale deposition. In another study, Naseri et al. (2015) obtained that injecting a sulfate-rich aqueous phase could result in significant precipitation and deposition of calcium sulfate and barium sulfate salts under favorable precipitation conditions. The authors also noticed a unique morphology of precipitated salts using scanning electron microscopy (SEM), which were different than those obtained from the experiments resulting in single salt precipitation and deposition. Note that most of the research work on inorganic scale precipitation and deposition associated with injected water incompatibility have been conducted in the context of smart, engineered, or low salinity waterflooding. The readers are encouraged to refer to the following papers that are selected from a significant number of articles in the literature on this subject (AlSofi et al. 2018; Dordzie and Dejam 2021; Fathi et al. 2012; Ghasemian et al. 2019; Olayiwola and Dejam 2020; Shirazi et al. 2019).

A significant part of the research work dedicated to inorganic scale formation and deposition, originated from incompatible water chemistry, is focused on predictive modeling and simulation with focusing on chemical reactions coupled with transport phenomena. Therefore, reactive flow modeling has been the main theme of several research studies. There are a few noteworthy studies on predicting sulfate scale formation and deposition based on empirical modeling and validation against experimental data (Moghadasi et al. 2006; Bedrikovetsky et al. 2009a, b). Other researchers used commercial software packages (Amiri et al. 2012; Hajirezaie et al. 2019) or molecular dynamics simulation approach (Kargozarfard et al. 2020) to evaluate scale formation and deposition. Chen et al. (2020) performed a set of experiments to evaluate barium sulfate scaling in sandstones, and concluded that the precipitation rate of barium sulfate is affected by several factors such as barium and sulfate ions' concentrations, temperature, and solution pH. These results were also confirmed by Haghtalab et al. (2015) who conducted similar experimental study on calcium sulfate scaling.

Use of geochemical software packages has become popular in recent years to handle a wide variety of chemical reactions in the aqueous phase in order to facilitate developing reactive fluid flow in porous media models (Abouie 2015; Chandrasekhar et al. 2018; Ozen 2017; Shabani et al. 2019a, b; Shabani et al. 2019a, b; Shirdel 2013). In such applications, it is required to couple a geomechanical model with a robust fluid flow in porous media model. However, there are some drawbacks associated with these earlier studies; for instance, only single salt precipitation is considered in some studies (Safari and Jamialahmadi 2014), and in others, some of the reactions are missing, or rock dissolution is ignored (Hajirezaie et al. 2019; Safari and Jamialahmadi 2014). In our opinion, there is a literature gap on developing a robust and straightforward modeling approach that covers reactive transport in porous media with focus on incompatibility of the aqueous phase chemistry between the injecting and in-situ fluids. This is an approach we have taken in this manuscript by developing a new water compositional model, where open-source MATLAB's Reservoir Simulation Toolbox (MRST) and PHREEQC software packages were used for fluid flow and aqueous phase geochemical calculations, respectively. The MRST is written in subject-oriented format and is customizable based on specific cases at hand (Lie 2019). In this paper, we first introduce all the assumptions associated with the proposed model. The governing equations of fluid flow and reactive transport, solved by numerical methods, are then presented in detail. The paper is then wrapped up with a sensitivity analysis performed using our proposed model with the aid of actual rock and fluid data.

Model description

In this study, we developed a new water compositional model, coupled with a geochemical module to support reactive transport in porous media associated with rock dissolution and salt precipitation and subsequent deposition because of the incompatible chemistry of the aqueous phases. There are several assumptions associated with this model development, listed below:

- At each time step, all the chemical reactions are in equilibrium.
- The reservoir is isothermal.
- All the scale masses formed at each grid block will deposit at the same grid block, i.e., the solid phase is immobile.
- Supersaturation of aqueous species is not allowed. If supersaturation occurs, mass of scale will be calculated in the geochemical module, and S.I. will be set to zero.
- Two immiscible and compressible phases of water and oil are considered. The proposed simulator contains a

compositional fluid flow model for the water phase, but the oil phase was treated as a “black oil” model, meaning that it is composed of a single component which is representative of all the oil components (Table 2).

- The volumetric concentration of deposited scale in each grid block is assumed to be equal to the change in porosity.
- The water phase contains nine components, including water, calcium ion, sodium ion, magnesium ion, strontium ion, barium ion, sulfate, carbonate and chloride.
- The salinity impact on water phase density is neglected.
- The equations are solved in a sequential implicit format, meaning that the transport equation is implicitly solved first, followed by solving the chemical reaction equations using the geochemical module.

Transport equations

A general system with N_p phases and N_c components is considered. The mass conservation equation for the component i is given by (Lie 2019):

$$\frac{\partial}{\partial t} \left[\sum_{\alpha=1}^{N_p} (\rho_{\alpha} \varphi x_{i,\alpha} S_{\alpha}) \right] + \nabla \cdot \left[\sum_{\alpha=1}^{N_p} (\rho_{\alpha} x_{i,\alpha} v_{\alpha} - \rho_{\alpha} D_i \nabla x_{i,\alpha}) \right] = q_i \tag{1}$$

where:

$$i \in \{O, W, Ca^{2+}, Na^{+}, Mg^{2+}, Sr^{2+}, Ba^{2+}, SO_4^{2-}, HCO_3^{-}, Cl^{-}\}$$

$$\alpha \in \{Water, Oil\}$$

In Eq. (1), x_i and D_i represent the mass ratio (i.e., component mass per 1 kg) of phase α and diffusion–dispersion tensor of component i in phase α , respectively, ρ_{α} , S_{α} and v_{α} are the density, saturation, and velocity of phase α , respectively.

In this study, sodium and chloride ions were assumed to be non-reacting components and always dissolved in the aqueous phase as they have no reaction in such a system whereas other ions such as calcium, strontium, barium, sulfate, hydrogen carbonate, and magnesium were assumed to be reacting components in the aqueous medium (Table 2). To evaluate the accuracy of the developed model, it is important to check the concentration profiles of the reacting and non-reacting components. This will be done using the following equations, that are used for calculating mass ratio of oil and water components:

$$x_{O,Oil} = 1, x_{O,Water} = 0$$

Table 2 Summary and description of the transport and geochemical models

# phases	# of components in the oil phase	# of components in the water phase	# of primary unknown variables	Well variables
2 (Oil, Water)	1 (oil)	9 (water, sodium, chloride, strontium, barium, calcium, sulfate, magnesium, hydrogen carbonate)	10 (pressure, saturation, and eight concentration values for each component in the water phase)	Based on the number of wells, a “well equation” will be added to the governing equations

$$x_{W,Oil} = 0, x_{W,Water} = 1$$

where $x_{O,Oil}$ and $x_{O,Water}$ represent mass of oil component per one kilogram of the oil and water phases, respectively; and $x_{W,Oil}$ and $x_{W,Water}$ represent mass of water component per one kilogram of the oil and water phases, respectively.

The phase velocity is determined by:

$$v_{\alpha} = -\frac{Kk_{r\alpha}(S_w)}{\mu_{\alpha}}(\nabla P_{\alpha} - \rho_{\alpha}g\nabla z) \quad (2)$$

where K , $k_{r\alpha}$, S_w , μ_{α} , P_{α} , g , and z stand for absolute permeability, relative permeability of phase α , water saturation, viscosity of phase α , pressure of phase α , gravity constant, and depth, respectively.

By expanding Eq. (1) for each component, ten advection–diffusion equations are obtained:

$$\frac{\partial}{\partial t}(\phi\rho_o(1 - S_w)) + \nabla \cdot (\rho_o v_o) = q_o \quad (3)$$

$$\frac{\partial}{\partial t}(\phi\rho_w S_w) + \nabla \cdot (\rho_w v_w) = q_w \quad (4)$$

$$\frac{\partial}{\partial t}(\phi\rho_w x_{i,Water} S_w) + \nabla \cdot (\rho_w x_{i,Water} v_w - \rho_w D\nabla x_{i,Water}) = q_i \quad (5)$$

where:

$$i = Ca^{2+}, Na^+, Mg^{2+}, Sr^{2+}, Ba^{2+}, SO_4^{2-}, HCO_3^-, Cl^-$$

There are ten unknown variables of pressure, saturation, and $x_{i,Water}$ for each dissolved component that need to be obtained by solving the advection–diffusion equations. The mass ratio parameter for each dissolved ion could be easily transformed into the concentration values. The pressure and flux conditions are defined below in Eqs. (6) and (7), respectively:

$$P(x = x_0, y = y_0, z = z_0, t) = cte \quad (6)$$

$$\frac{\partial P}{\partial x} = cte, \frac{\partial P}{\partial y} = cte, \frac{\partial P}{\partial z} = cte \quad (7)$$

The governing equations represented by Eqs. (3) to (5) were then solved using the initial and boundary conditions expressed in Eqs. (6) and (7), respectively, after being discretized and linearized using finite difference method. There is a source/sink variable for each component in Eqs. (3) to (5). These expressions were modified by a well equation (Lie 2019), which is given for a single grid using the following expression:

$$q_{i,\alpha} = \rho_i x_{i,\alpha} T\gamma(P_{\alpha} - P_{bh} - \rho_i g \Delta h) \quad (8)$$

where T , γ , and Δh are well productivity/injectivity index, mobility of phase α , and true vertical depth of the well, respectively.

The nonlinear Eqs. (3) to (5) were solved implicitly using Newton's method. These equations were discretized and transformed into linear system of equations through defining them in a new physical model. The linear system of equations in the new physical model was then solved considering the initial and boundary conditions. By solving the transport model in each timestep, several parameters were obtained including pressure, saturation, and concentration of sulfate, strontium, barium, calcium, chloride, sodium, hydrogen carbonate, and magnesium ion.

Geochemical model

PHREEQC is a geochemical software capable of modeling many reactions between water and inorganic minerals. To use this software in scripting languages, PHREEQC has been implemented in a module, known as IPHREEQC, which can easily be coupled with other software packages (Charlton and Parkhurst 2011). In this study, IPHREEQC module was used to set up and solve the geochemical model. It was assumed that all reactions are at equilibrium state. In addition, calcite surface complexation reactions were considered. A comprehensive study on surface complexation reactions associated with calcite and quartz surfaces was published by Mahani et al. (2016) (Table 3). With reference to this study, we considered two surface binding sites of calcium bind and carbonate bind for the calcite surface. All the dissolution/precipitation and surface complexation reactions are presented in Table 3.

The geochemical module set up in our study calculates the equilibrium concentrations and amounts of solid particles based on the solid's S.I. values. Since the equilibrium constants of these reactions are functions of temperature, the Van't Hoff model was used to calculate the equilibrium constant-temperature relation (Charlton and Parkhurst 2011). The S.I. value for each reaction was first calculated based on the concentration of each solid phase in the dissolution reactions (Wu 2018):

$$S.I. = \log\left(\frac{IAP}{K_{eq}}\right) \quad (9)$$

where IAP and K_{eq} are ion activity and solubility products, respectively.

The S.I. formula for anhydrite formation reaction is expressed as:

$$S.I. = \log\left(\frac{(a_{Ca^{2+}})(a_{SO_4^{2-}})}{K_{eq}}\right) \quad (10)$$

Table 3 List of dissolution/precipitation and surface complexation reactions from PHREEQC database (Parkhurst and Appelo 1999) and Mahani et al. (2016), respectively

Dissolution/Precipitation reactions		
1	$CaSO_{4(s)} \rightleftharpoons Ca_{(aq)}^{2+} + SO_{4(aq)}^{2-}$	$\log K = -4.36^A @ 25^\circ C$
2	$StrSO_{4(s)} \rightleftharpoons Ba_{(aq)}^{2+} + SO_{4(aq)}^{2-}$	$\log K = -6.63^A @ 25^\circ C$
3	$BaSO_{4(s)} \rightleftharpoons Ba_{(aq)}^{2+} + SO_{4(aq)}^{2-}$	$\log K = -9.97^A @ 25^\circ C$
4	$CaSO_4 \cdot 2H_2O_{(s)} \rightleftharpoons Ca_{(aq)}^{2+} + SO_{4(aq)}^{2-} + 2H_2O_{(l)}$	$\log K = -4.58^A @ 25^\circ C$
5	$CaCO_{3(s)} \rightleftharpoons Ca_{(aq)}^{2+} + CO_{3(aq)}^{2-}$	$\log K = -8.48^A @ 25^\circ C$
6	$CaMg(CO_3)_{2(s)} \rightleftharpoons Ca_{(aq)}^{2+} + Mg_{(aq)}^{2+} + CO_{3(aq)}^{2-}$	$\log K = -16.54^A @ 25^\circ C$
Surface complexation reactions		
7	$> CaOH + H^+ \rightleftharpoons CaOH_2^+$	$\log K = 11.8^B @ 25^\circ C$
8	$> CaOH + HCO_3^- \rightleftharpoons CaCO_3^- + H_2O$	$\log K = 5.8^B @ 25^\circ C$
9	$> CaOH_2^+ + SO_4^{2-} \rightleftharpoons CaSO_4^- + H_2O$	$\log K = 2.1^B @ 25^\circ C$
10	$> CO_3H \rightleftharpoons CO_3^- + H^+$	$\log K = -5.1^B @ 25^\circ C$
11	$> CO_3H + Mg^{2+} \rightleftharpoons CO_3Mg^+ + H^+$	$\log K = -1.7^B @ 25^\circ C$
12	$> CO_3H + Ca^{2+} \rightleftharpoons CO_3Ca^+ + H^+$	$\log K = -2^B @ 25^\circ C$

Each new Ca^{2+} and SO_4^{2-} concentrations should be calculated at equilibrium condition. Since a S.I. value of zero represents equilibrium condition, these new concentrations were calculated at zero S.I. value. By calculating new ion concentrations, determining the amounts of precipitated particles in the water phase became feasible.

To set up the geochemical model, the following procedure was followed: First, the aqueous solution, its pressure, temperature and pH were defined, along with the aqueous phase density and its ionic concentration. Then, all the salts and chemical reactions associated with their production, along with the equilibrium parameters should be defined based on the library content of the software package (Table 3). In this study, five solid compounds of anhydrite, celestite, barite, dolomite, and calcite were included in the system, and the amount of each solid compound was calculated based on the equilibrium constant(s) associated with their formation reaction. In addition, the target S.I. value and initial amount of each solid compound were defined. When the calculated S.I. value for each solid compound became equal or greater than that of the defined target value, the compound was considered to have the precipitation and deposition potential. At the end, the geochemical module calculated the equilibrium state of the defined aqueous solution.

Solid deposition, rock dissolution and permeability impairment models

The solid deposition, rock dissolution and their impact on the porosity and permeability changes are calculated using the equations listed in Table 4.

For the porosity change due to solid deposition or rock dissolution, a simple material balance can be done assuming that the solid phase is immobile. In Eq. (11), V_{scales} represents rock dissolution (with a negative value) or scale deposition

Table 4 Effect of solid deposition and dissolution on the porosity and permeability changes, represented by analytical models/correlations

Porosity impairment model	
	$\varphi = \varphi_0 - \left(\frac{V_{scales}}{V_{bulk}} \right) \quad (11)$
Permeability impairment model	
Carman-Kozeny model	$\frac{K}{K_0} = \left(\frac{\varphi}{\varphi_0} \right)^3 \left(\frac{1-\varphi_0}{1-\varphi} \right)^2 \quad (12)$
Civan model (First)	$\frac{K}{K_0} = \frac{F_s \tau_0}{F_s \tau} \left(\frac{S_v}{S_v} \right)^2 \left(\frac{\varphi}{\varphi_0} \right)^3 \quad (13)$
Civan model (Second)	$\frac{K}{K_0} = \frac{F_s \tau_0}{F_s \tau} \left(\frac{\varphi}{\varphi_0} \right)^2 \quad (14)$
Shutong and Sharma model	$\frac{K}{K_0} = \frac{1}{1+\beta(\varphi_0-\varphi)} \quad (15)$

(with a positive value). For permeability impairment, several models have been introduced including (a) Kozeny-Carman model, shown by Eq. (12) (Alpak et al. 1999); (b) Civan models, represented by Eqs. (13) and (14) (Civan 2016) in which F_s , τ , and S_v are shape factor, tortuosity, and pore surface per unit bulk volume, respectively, and c) Shutong and Sharma model (Shutong and Sharma 1997), shown by Eq. (15) in which β is formation damage factor, an empirical coefficient. For simplicity, it was assumed that the deposit concentration equals the porosity change whereas in reality, the porosity change is more than the deposit concentration. In this study, we used all these four permeability impairment models to predict permeability damage due to scale deposition.

Reactive transport model workflow

Inspired by ad-eor and ad-blackoil modules (Lie 2019), we developed the so-called ad-scale module based on the transport equations, geochemical relations and porosity/permeability impairment models mentioned in sections "Transport

equations", "Geochemical model" and "Solid deposition, rock dissolution and permeability impairment models". A new sub-class, called *OilWaterScaleModel*, and some new functions, listed in Table 5, were also developed in the open-source MRST environment and are freely available online (refer to the "Data and Computer code availability" subsection at the end of this manuscript).

The *OilWaterScaleModel* sub-class was coupled with IPHREEQC through the IPhreeQC function, which was designed for coupling the geochemical model with the fluid flow model. In Fig. 1, the general workflow for the coupled model is presented. At each timestep, first, the transport equation is solved implicitly. Moving to the geochemical model, the amounts of scales, rock dissolution, and ion concentration for each component at the equilibrium state are calculated. At the end, porosity and permeability are updated according to the impairment models. This loop is then repeated until the last timestep.

Further details on the geochemical and transport models are also illustrated in Fig. 2. Starting on the fluid flow model, the input data including grid information, rock model, fluid model, wells, boundary conditions, initial condition, and time schedule are first defined by the user. The transport model (Eqs. (3) to (5)) is solved implicitly in one timestep, and following convergence at each timestep, all variables at $t + \Delta t$ are calculated and stored in the *states* matrix that

Table 5 Added functions

New functions

BariumComponent
SulfateComponent
CalciumComponent
StrontiumComponent
CarbonateComponent
SodiumComponent
MagnesiumComponent
ChlorideComponent
OilWaterScaleModel
validateState
getEquations
equationsOilWaterScale
getVariableField
getComponentNames
addComponentContributions
getExtraWellContributions
getExtraWellPrimaryVariableNames
getExtraWellEquationNames
IPhreeQC
CoreDataProcess
ReservoirDataProcess
WellDataProcess

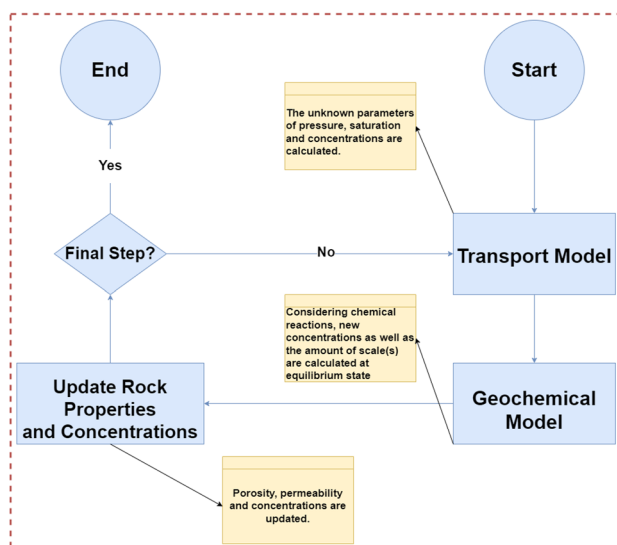


Fig. 1 General workflow of the coupled fluid flow and geochemical model

includes flow variables. The mass ratio values are converted to concentration values, which are then transported along with the pressure values to the geochemical model at the given pressure of each grid when the temperature is assumed constant. In the geochemical model, the ions concentration values are calculated along with amounts of scale formation and rock dissolution at the equilibrium condition. The *states* matrix and rock properties will then be updated based on the geochemical model's output. The ion concentration values are converted to mass ratio ($x_{i,Water}$) and updated in the *states* matrix. The porosity for each grid block is updated based on the scale volume, which also triggers another correction in permeability of each grid block based on the permeability impairment model(s). The loop will then be repeated at a new timestep until the end of the simulation process.

Results and discussion

In order to validate the performance of our proposed coupled fluid flow-geochemical model, we present a benchmarking process in section "Benchmarking the proposed coupled simulator" through which we first compare our coupled model's predictions against an experimental study. In addition, we check our model's predictions against another simulation study conducted using a known simulator (i.e., UTCHEM-IPHREEQC coupled model) to check the accuracy of our model's predictions as well as to validate its performance. Once confirmed, our proposed coupled simulator was used to model a series of core-scale and field-scale cases to assess the risks of scale formation and deposition associated with incompatible water injection in carbonate formations. These

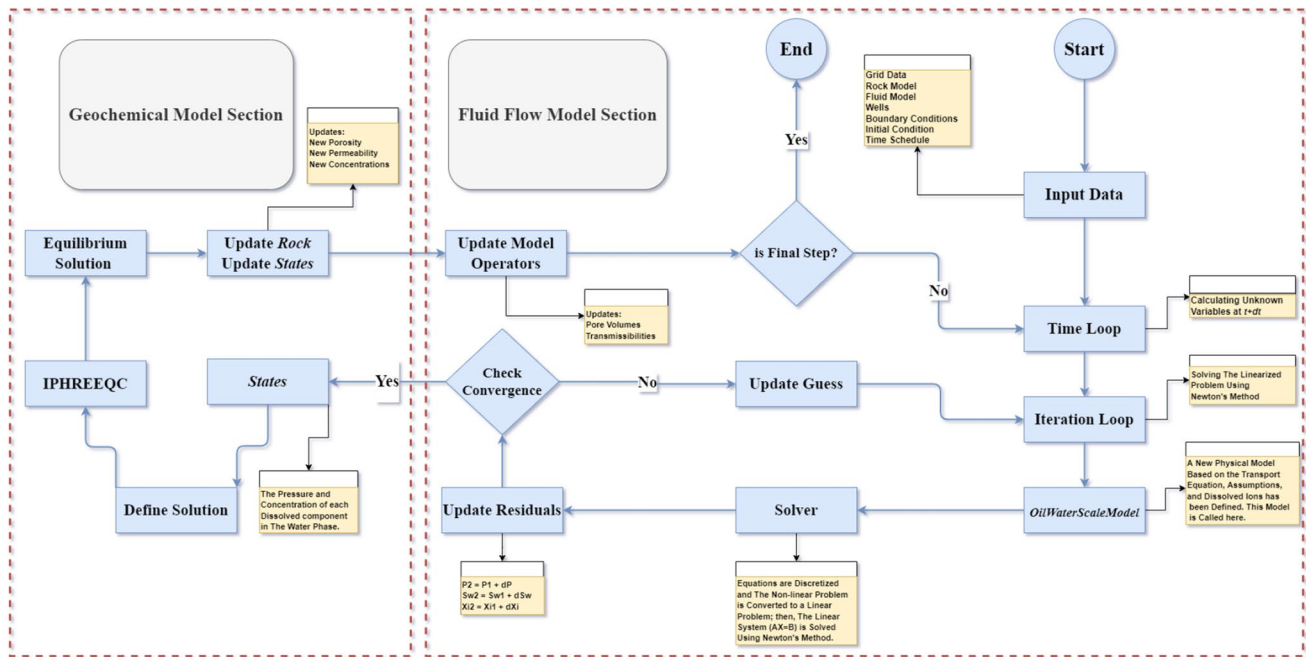


Fig. 2 Further details on the coupled geochemical and fluid flow / transport model

Table 6 Rock properties from coreflooding test reported by Chandrasekhar et al. (2018)

Porosity (%)	Permeability (mD)	Length (cm)	Diameter (cm)	Mineralogy
17	25	15.3	3.8	Calcite

Table 7 Composition of injected brine from coreflooding test reported by Chandrasekhar et al. (2018)

Concentration	Na	Cl	Mg	Ca	SO ₄
In-situ brine (ppm)	40,288	107,309	2,815	11,236	215
Injecting brine (ppm)	12,892	26,578	1,519	507	3,485

case studies are presented in sections "Coupled simulation of fluid flow and reactive transport: a sensitivity analysis on the injected water composition" and "Field-scale numerical simulation of reactive flow: an offshore carbonate reservoir case study".

Benchmarking the proposed coupled simulator

To validate the proposed coupled simulator, a coreflooding study performed by Chandrasekhar et al. (2018) was selected. The coreflooding experiment included a single-phase brine injection at a test temperature of 393 K, an injection flow rate of 0.02 mL/min, and production pressure of 55 psia. The injected brine phase contained five dissolved components of sodium, chloride, sulfate, calcium and magnesium. The rock and fluid properties for this coreflooding test are listed in Tables 6 and 7, respectively. At the effluent, the concentration of each component was measured using an ion chromatograph. Since all the ions used in the in-situ and injecting brine phases in this coreflooding test are included in the coupled simulator we developed in the current study, use of this

coreflooding experiment to validate our model's performance seems appropriate.

The concentration of reacting and non-reacting dissolved ions at the effluent were computed with our proposed coupled model. We used the reactions' equilibrium constants as well as dispersion-diffusion coefficient(s) as tuning parameters to match the experimental data of ion concentrations at the effluent. A constant value of $10^{-11} m^2/s$ for the diffusion coefficient proved to be the best value to get the closest match to the experimental data. We also used the Van't Hoff correlation in order to compute the reactions' equilibrium constants which resulted in the closest match to the experimental data. A list of the tuning parameters and their values are presented in Table 8. The relative error and R^2 values were determined using the following Eqs:

$$\text{Relative Error} = \left| \frac{C_{\text{Actual}} - C_{\text{Predicted}}}{C_{\text{Predicted}}} \right| * 100 \quad (16)$$

Table 8 Tuning parameters for the coupled simulation model during the benchmarking stage

Component	Diffusion coefficient (m ² /s)	Relative error in concentration prediction (%)	<i>a</i> for concentration prediction
SO ₄ ²⁻	1e-11	16.5	0.927
Ca ²⁺	1e-11	1.7	0.999
Mg ²⁺	1e-11	8.5	0.912
Na ⁺	1e-11	7.1	0.971
Cl ⁻	1e-11	17.2	0.923
Reaction			Tuned Equilibrium Constants at 393 K
CaSO _{4(s)} ⇌ Ca _(aq) ²⁺ + SO _{4(aq)} ²⁻			log K = -5.600
SrSO _{4(s)} ⇌ Ba _(aq) ²⁺ + SO _{4(aq)} ²⁻			log K = -7.5287
BaSO _{4(s)} ⇌ Ba _(aq) ²⁺ + SO _{4(aq)} ²⁻			log K = -9.5825
CaSO ₄ ·2H ₂ O _(s) ⇌ Ca _(aq) ²⁺ + SO _{4(aq)} ²⁻ + 2H ₂ O _(l)			log K = -4.9796
CaCO _{3(s)} ⇌ Ca _(aq) ²⁺ + CO _{3(aq)} ²⁻			log K = -9.5875
CaMg(CO ₃) _{2(s)} ⇌ Ca _(aq) ²⁺ + Mg _(aq) ²⁺ + CO _{3(aq)} ²⁻			log K = -17.0900

$$R^2 = 1 - \frac{\text{RSS}}{\text{TSS}} \quad (17)$$

where C_{Actual} , $C_{\text{Predicted}}$, RSS, and TSS are actual concentration (i.e., measurement), predicted concentration by our model, sum of squares of residuals, and total sum of squares, respectively.

In addition to the experiments, Chandrasekhar et al. (2018) also coupled UTCHEM fluid flow simulator with IPHREEQC geochemical model, and attempted to match their experimental data with this coupled simulation model. In Figs. 3, 4, 5, 6 and 7, the experimental and simulation results by Chandrasekhar et al. (2018) are presented, along with the predicted results using our proposed coupled simulation model, referred to as “ad-scale” model in this paper. In these figures, the normalized concentrations of target ions at the effluent are plotted as a function of dimensionless time. The exemplary performance of the ad-scale model to predict the “S style” trends of the experimental data is evident from the two statistical parameters defined for these predictions, namely the coefficient of determination and absolute error. The biggest discrepancy between the measured and predicted ion concentrations appears to be for the case of Chloride ion (Fig. 4) with a relative error of 17.2% between the ad-scale predictions and experimental data. As seen in this figure, the UTCHEM-IPHREEQC coupled model also had the highest discrepancy when compared to the experimental data for the case of Chloride ion. According to Chandrasekhar et al. (2018), the reason was due to the malfunction of the ion chromatograph used in their study to measure high concentrations at the effluent, which resulted in erroneous experimental data for the specific case of Chloride ion that had some of the biggest effluent concentrations.

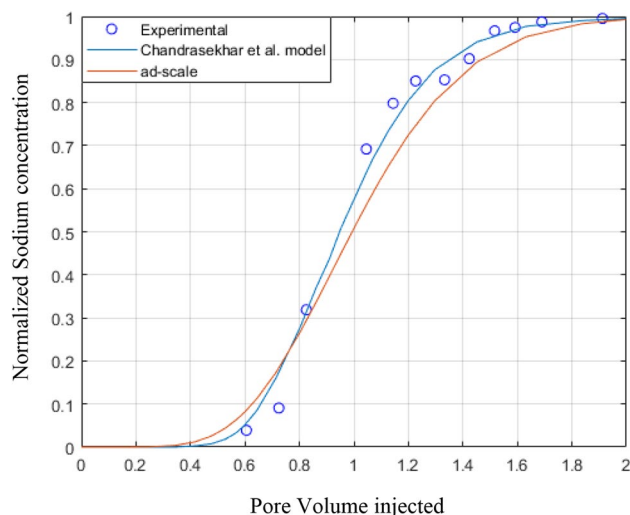


Fig. 3 Comparison of the measured versus predicted *Sodium concentration* at the coreflooding outlet. The R^2 and Relative Error associated with ad-scale model predictions compared to the experimental data are 0.971 and 7.1%, respectively

Therefore, the Chloride ion experimental data reported in this reference are not considered reliable, and no conclusion can be drawn based on the Chloride ion concentration predictions using our proposed couple model. However, the Sodium, Magnesium, Calcium and Sulfate concentrations at the coreflooding outlet were predicted with high accuracy using ad-scale coupled model. The accuracy of predictions using ad-scale model can be qualitatively compared to that of the UTCHEM-IPHREEQC coupled model used by Chandrasekhar et al. (2018), and it is evident that these two models are relatively the same when predicting

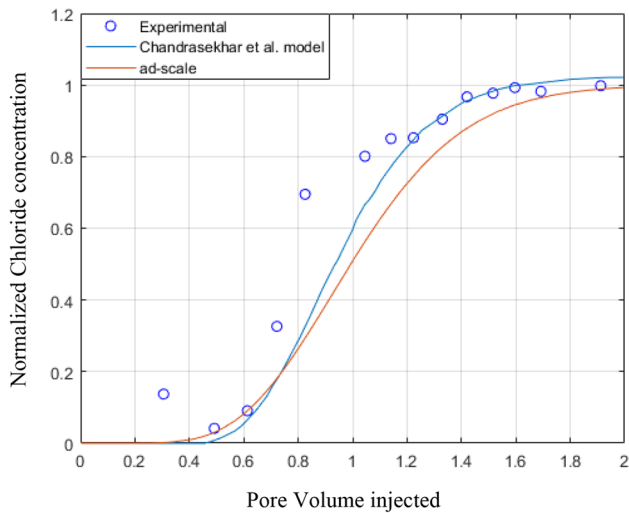


Fig. 4 Comparison of measured versus predicted *Chloride concentration* at the coreflooding outlet. The R^2 and Relative Error associated with ad-scale predictions compared to the experimental data are 0.923 and 17.2%, respectively

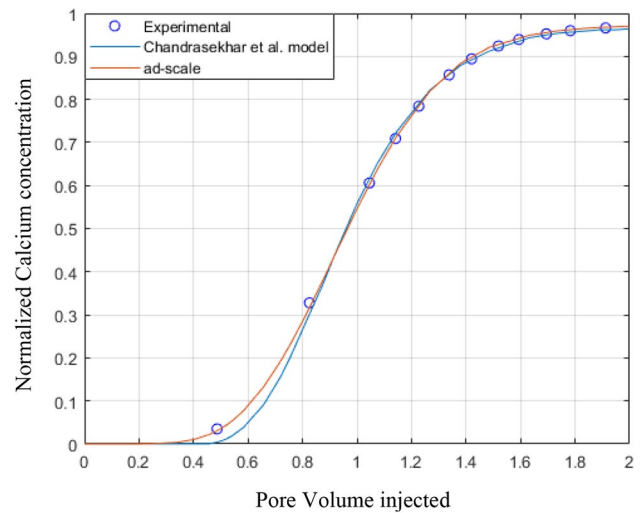


Fig. 6 Comparison of measured versus predicted *Calcium concentration* at the coreflooding outlet. The R^2 and Relative Error associated with ad-scale model predictions compared to the experimental data are 0.999 and 1.7%, respectively

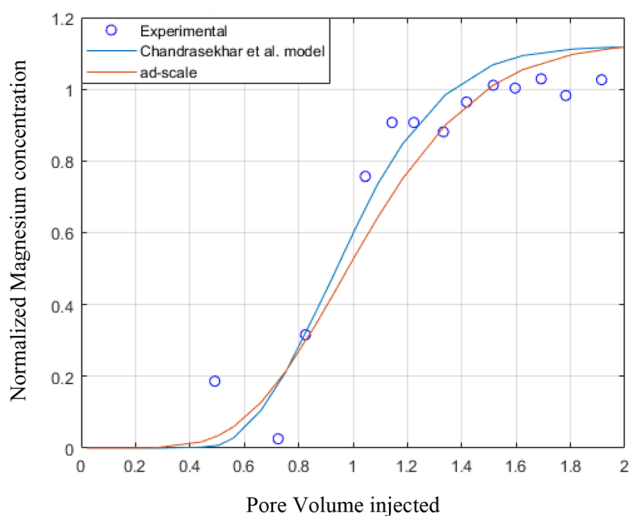


Fig. 5 Comparison of measured versus predicted *Magnesium concentration* at the coreflooding outlet. The R^2 and Relative Error associated with ad-scale model predictions compared to the experimental data are 0.912 and 8.5%, respectively

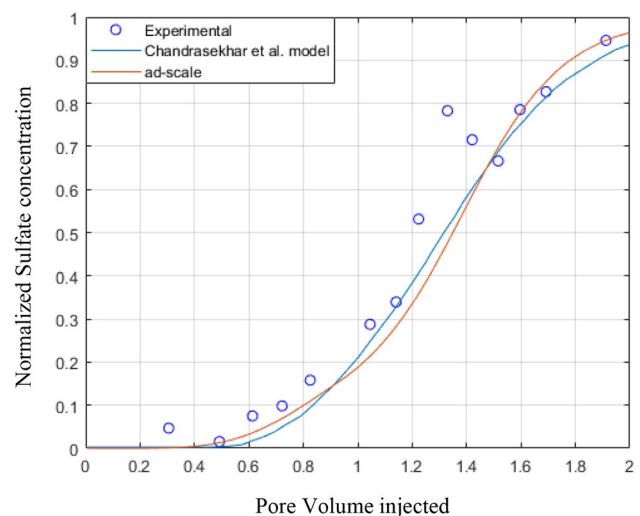


Fig. 7 Comparison of measured versus predicted *Sulfate concentration* at the coreflooding outlet. The R^2 and Relative Error associated with ad-scale model predictions compared to the experimental data are 0.927 and 16.5%, respectively

the ion concentrations. Note that in Figs. 4 and 5, some of the models' predictions as well as calculated normalized concentrations based on concentration measurements have values more than 1.0, which are physically unfeasible and could be attributed to some unknown measurement and modeling errors.

Depending on the defined fluid and rock system, some ions are considered “reacting” while others are assumed to be “non-reacting”. In the reactive transport case reported by

Chandrasekhar et al. (2018), for instance, Sodium is considered a “conservative non-reacting” component while Sulfate is assumed to be “non-conservative reacting” component which can adsorb to the rock surfaces in the form of solid scale. Therefore, Sulfate concentration at the effluent might suffer a loss compared to the non-reacting ions that are not retained by the porous structure. In Fig. 8, the normalized Sodium, Calcium and Sulfate concentrations at the effluent are plotted versus dimensionless time. The loss in Sulfur

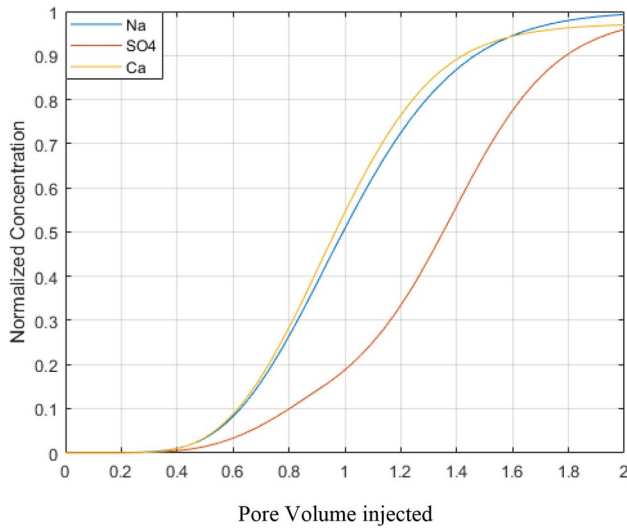


Fig. 8 Normalized effluent concentration as a function of dimensionless time

content at the effluent compared to a non-reacting component such as Sodium at similar time intervals is evident, which shows the reactive nature of Sulfate toward anhydrite formation. In other words, Sulfur concentration might reach that of a non-reacting component (such as Sodium) with a significant delay, or might not catch up at all due to the consumption along the flow path length, as is the case in Fig. 8. The case of Calcium is more complex. While it is a reactive component, its concentration profile in the aqueous phase at the effluent is similar to a non-reacting component (i.e., Sodium). The reason could be the combined consumption and generation of Calcium ion along the flow path length due to CaSO_4 formation and calcite mineral dissolution by the injecting water phase, respectively, that could impose a balance upon Ca concentration over the full injection duration.

Table 11 Change in the injecting water composition by adjusting the mixing ratio between FW and SW

Simulation Run ID	FW:SW mixing ratio
S1	0:1
S2	1:3
S3	1:1
S4	3:1

Coupled simulation of fluid flow and reactive transport: a sensitivity analysis on the injected water composition

Once the developed ad-scale model was validated in section "Benchmarking the proposed coupled simulator", it was used to investigate the effect of injecting water composition on scale deposition at the core-scale. The injecting water composition was changed by defining a series of scenarios in which a mixture of the injecting and in-situ water with predetermined mixing ratios were injected into the core. The composition of in-situ aqueous phase, called formation water (FW) in this paper, as well as that of the injected seawater (SW) are borrowed from the literature (Payehghadr and Eliasi 2010) and described in Table 9. Four coreflooding processes were simulated using the ad-scale coupled model to determine the effect of mixing ratio on changes in rock properties. The porous medium selected for these core-scale simulation cases is a carbonate rock with properties borrowed from the literature (Payehghadr and Eliasi 2010), and the rock properties as well as endpoint relative permeability and saturations are shown in Table 10. To investigate the effect of FW/SW mixing ratio, four scenarios were defined (Table 11). In Table 12, other rock and fluid properties needed for the simulation study of these four scenarios are presented.

Assuming that all the scales formed in each grid block has the “deposition” potential within the same grid block, the volumetric contribution of scales formed per core length were calculated, and the porosity values were reduced accordingly to account for the scale-induced porosity impairment (Fig. 9). The porosity impairment occurred mainly

Table 9 FW and SW composition

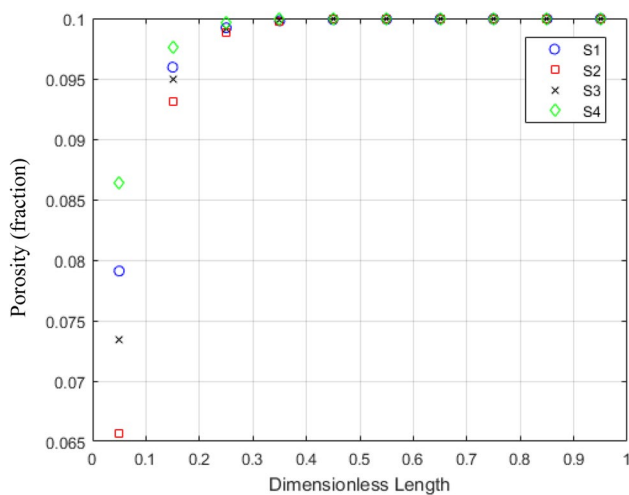
Concentration (ppm)	Component							
	Na	HCO ₃	Cl	Mg	Ca	SO ₄	Sr	Ba
FW	70,015	5	129,022	1701	9500	220	200	5
SW	8195	157	20,955	1306	564	2498	0	0

Table 10 Rock properties and endpoints

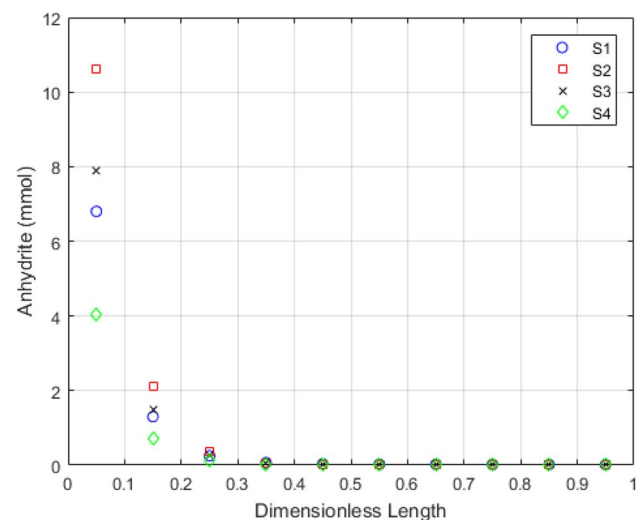
Property	$k_{ro,max}$	$k_{ro,min}$	$k_{rw,max}$	$k_{ro,min}$	Sw_i	Sw_{ir}	So_{ir}	$\Phi(\%)$	K (mD)
Value	0.45	0	0.25	0	0.32	0.27	0.28	10	9

Table 12 Simulation input data

Parameter	Value
Grid number	20*1*1
Grid block size (cm ³)	0.765*3.37*3.37
Operating pressure (MPa)	0.692
Operating temperature (K)	393
Initial core porosity (%)	10
Initial core permeability (mD)	9
Initial water saturation (fraction)	0.26
Water viscosity (cP)	0.5
Water compressibility Pa ⁻¹	1.45e-10 Pa ⁻¹
Water density (kg/m ³)	1,100
Oil viscosity (cP)	4
Oil compressibility (Pa ⁻¹)	8.70e-10
Oil density (kg/m ³)	800
Rock compressibility (Pa ⁻¹)	1.45e-10
Injection flow rate (cc/hr)	3.13
Injection duration (Dimensionless, PV injected)	10
Formation water injection duration (Dimensionless, PV injected)	2
Incompatible water injection duration (Dimensionless, PV injected)	8

**Fig. 9** Porosity profile, in volume fraction, along the core length

over the first 20% of the core's frontend length, particularly at about 5% dimensionless distance from the core frontend, which is related to the grid block associated with the injection spot. Among the four simulation cases, S2 with minimum FW/SW mixing ratio of 1:3 resulted in the most severe porosity reduction of about 35% of its original amount. Looking into the Anhydrite precipitation profile at the end of the injection process (i.e., 10 PV injected) in Fig. 10, the porosity decline could be clearly related to the Anhydrite formation and deposition, as a major sulfate scale, at the core frontend. The permeability damage due to scale deposition was also calculated using four analytical models for all the

**Fig. 10** Anhydrite formation profile at the end of coreflooding

coreflooding scenarios (Figs. 11, 12, 13 and 14). The Civan models provided conservative permeability impairment predictions while the Shutong and Sharma model predicted the steepest decline in permeability as a result of scale deposition. Note that the predicted permeability values were the harmonic averaged permeability reduction along the core length. The Shutong and Sharma model depends on the formation damage factor, which should be determined experimentally. For the purpose of these simulation cases, β was assumed to be 50.

During incompatible water injection into a surface-active porous medium such as a carbonate core, it is expected that

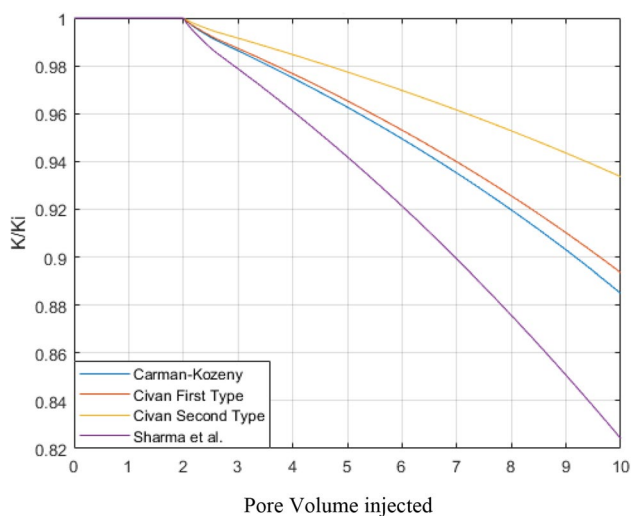


Fig. 11 Permeability impairment due to scale formation and deposition during SW injection from 2 to 10 PV injection period for S1 coreflooding scenario

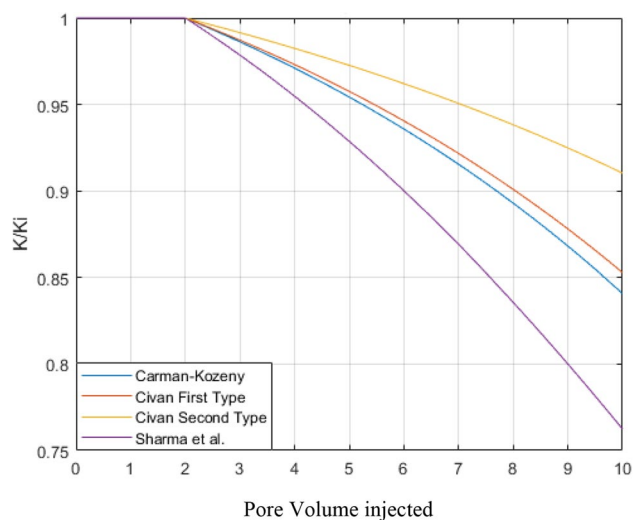


Fig. 13 Permeability impairment due to scale formation and deposition during SW injection from 2 to 10 PV injection period for S3 coreflooding scenario

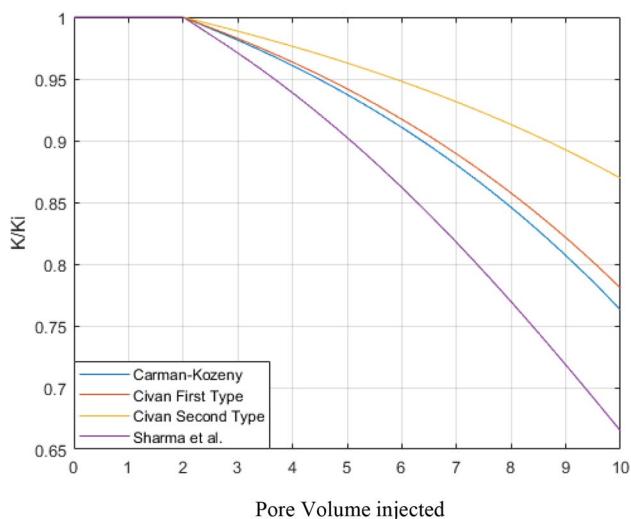


Fig. 12 Permeability impairment due to scale formation and deposition during SW injection from 2 to 10 PV injection period for S2 coreflooding scenario

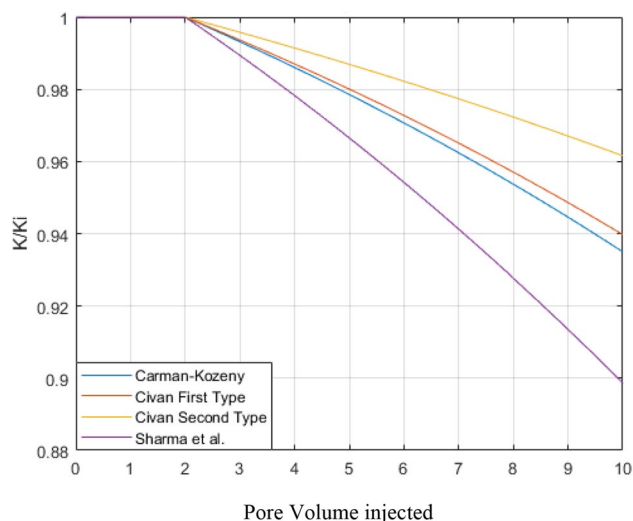


Fig. 14 Permeability impairment due to scale formation and deposition during SW injection from 2 to 10 PV injection period for S4 coreflooding scenario

calcite would be dissolved in the injected aqueous phase. It is also expected to observe dolomitization process in such circumstances. Our simulation results confirmed these hypotheses. According to Fig. 15, the calcite dissolution increases when approaching the frontend part of the core, close to the injection spot. However, this rock dissolution into the injected aqueous phase is diminished moving along the flow path length toward the production end, and mainly no calcite dissolution occurs after a dimensionless length of about 0.3 between the four simulated coreflooding cases. As expected, the greatest calcite dissolution values are

associated with simulation case S1 and S2, with the smallest FW/SW ratio on the injection side. Note that Calcium concentration in the injecting aqueous phase was among the smallest values for these two mixing ratios compared to the rest of scenarios, which triggers such calcite dissolution from the rock texture into the injecting aqueous phase. The negative calcite content values on the y-axis in Fig. 15 indicate rock dissolution. On the other hand, a dolomitization process is expected when such calcite dissolution occurs. As observed in Fig. 15, the dolomite concentration increases when approaching the frontend of the flow length, which is

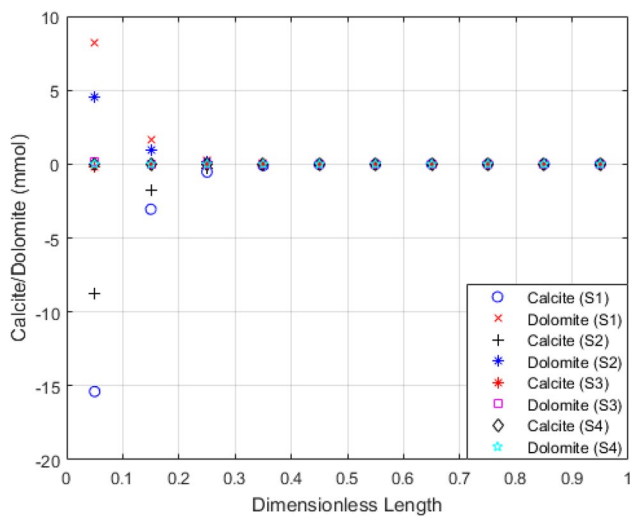


Fig. 15 Calcite dissolution and dolomite formation profiles along the flow path length at the end of the water injection process (i.e., 10 PV injected)

in agreement with the trend observed for the calcite content. Our model suggests that in all coreflooding cases, both the scale formation and rock dissolution happen in the regions close to the injection side.

Field-scale numerical simulation of reactive flow: an offshore carbonate reservoir case study

One of the main outcomes of reactive flow in porous media at the field-scale, associated with incompatible water injection, is the loss of injectivity due to scale formation and deposition. Moghadasi et al. (2004) studied the injectivity decline of a carbonate reservoir under waterflooding, and realized that a 75% reduction in seawater injection occurred over a seven-year injection period. In the absence of rock and fluid properties to implement a detailed field-scale coupled reservoir simulation, we conducted a dimensionless comparison approach in which the predicted injection flow rates are normalized between the values of zero and 1, with zero and 1 standing for no injection flow rate and the greatest injection flow rate value, respectively. To quantitatively predict the actual formation damage caused by incompatible water injection, it is required to have detailed rock and fluid

properties. However, it is only needed to have the formation water and seawater composition data, as indicated in Table 13, in order to perform the comparative dimensionless approach to illustrate loss of injectivity. Through successful prediction of the field-scale injection flow rates, the ad-scale model was tuned for this particular field-scale simulation case, and the tuned model was then used to predict changes in reservoir quality (i.e., porosity and permeability) over time, for which no actual field-scale measurements are available.

In the absence of any rock, fluid and production data, the only available data for history match in this reservoir is water injection rate. Assuming that loss of injectivity is directly related to the inorganic scale deposition in this reservoir, the formation damage factor was used as the tuning parameter in this history matching exercise, and the best value of this fitting parameter was obtained at $\beta = 994$ based on a sensitivity analysis / minimization done on the relative error associated with predicting the water injection rate with respect to the actual field-scale injection data (Fig. 16). According to this error minimization approach, the water injection flow rate could be predicted with an average relative error of about 9.02% on a field-scale basis (Figs. 16 and 17), which resulted in a very good agreement between the

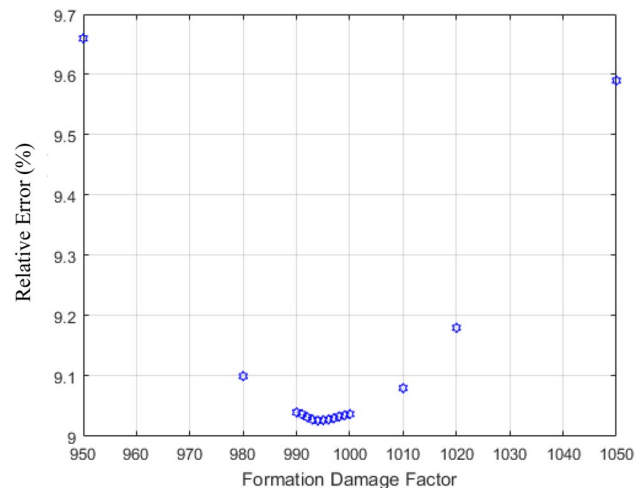


Fig. 16 Sensitivity analysis on average relative error associated with predicting field-scale water injection flow rate as a function of the tuning parameter (i.e., formation damage factor)

Table 13 Composition of various aqueous phases used in field-scale simulation study

Concentration (ppm)	Component							
	Na	HCO ₃	Cl	Mg	Ca	SO ₄	Sr	Ba
Formation Water	37,128	350	73,248	485	7,843	125	0	0
Seawater	9720	200	20,955	1306	75	3240	0	0
Low Salinity Water	2807	112	5432	323	403	934	0	0
River Water	285	152	418	43	141	471	6	0

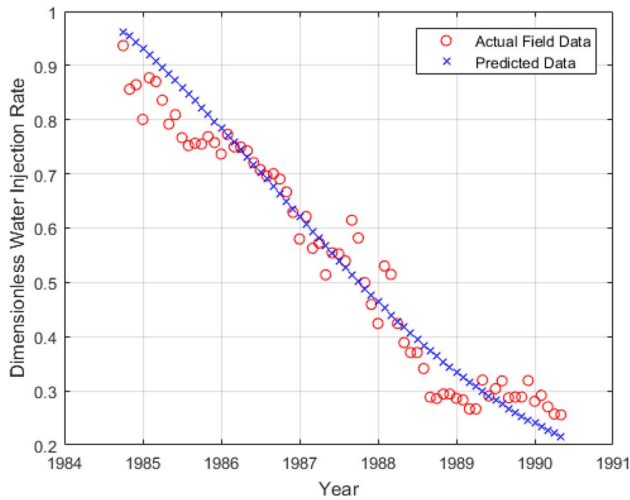


Fig. 17 Predicted versus field-scale water injection rates in the target reservoir over a seven-year period at optimum formation damage factor obtained from Fig. 18

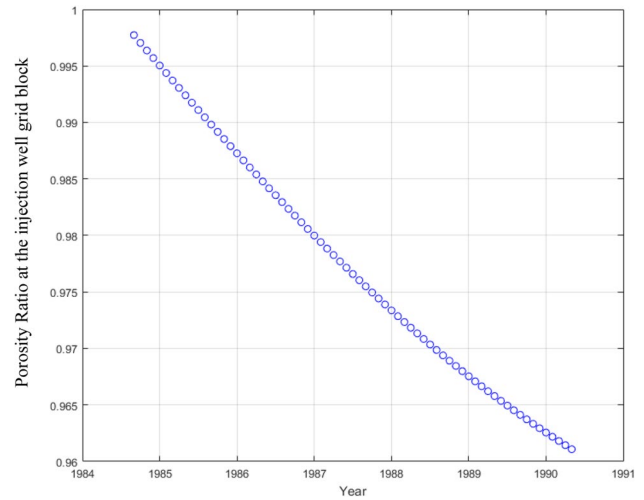


Fig. 19 Predicted porosity ratio in the grid block associated with the injection well during seawater injection

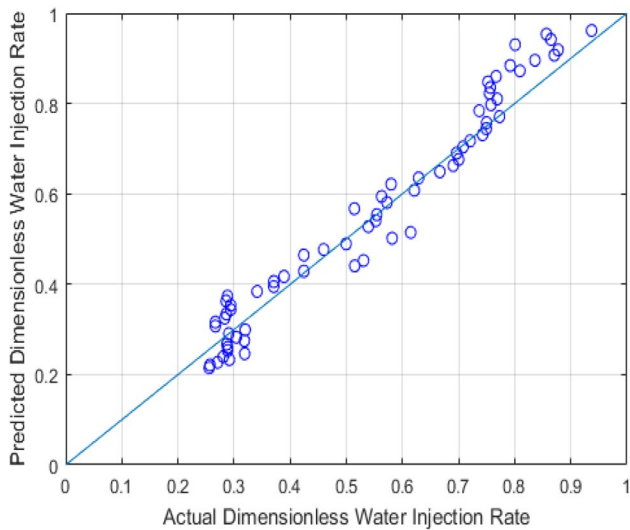


Fig. 18 Parity plot comparing the predicted versus actual dimensionless water injection rates at optimum formation damage factor that resulted in the most accurate predictions

predicted and actual water injection flow rates with a coefficient of determination of about $R^2 = 0.99$ (Fig. 18).

After the coupled model was tuned for this particular field-scale case through proper prediction of the dimensionless water injection flow rates, we extracted more data from this tuned model with respect to changes in reservoir quality by time during seawater injection (Fig. 19 and 20). From section "[Coupled simulation of fluid flow and reactive transport: a sensitivity analysis on the injected water composition](#)", a major drop in porosity occurs at the grid block(s) associated with the injection well area. Only a 4% decline in porosity was achieved at the injection spot

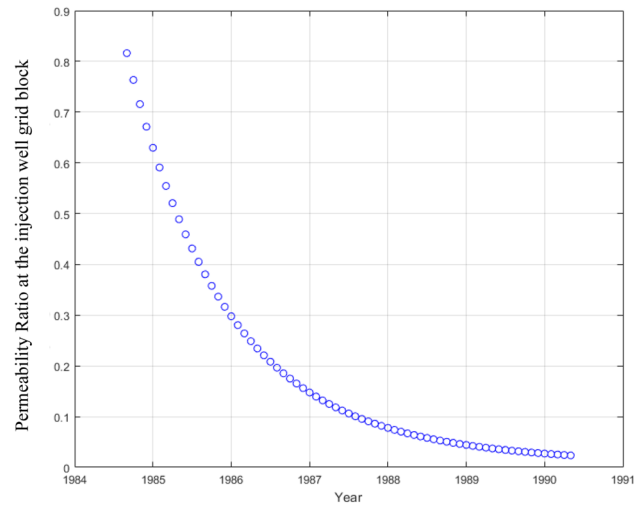


Fig. 20 Permeability ratio in the grid block associated with the injection well during seawater injection

over the seawater injection period (Fig. 19). However, the permeability decline at the injection well grid block was significant over the same time period, resulting in almost complete blockage of the injection site (Fig. 20). Note that these findings are achieved under primary assumptions based on which the as-scale coupled simulator was designed, that all the scales formed at each particular grid block are assumed to have the “deposition potential”, and also deposit within the same grid block, i.e., no movement of scales are allowed through the porous medium. Since the fluid flow near the wellbore area has a radial pattern, any changes in the near wellbore permeability significantly affect the well injectivity (Fig. 21).

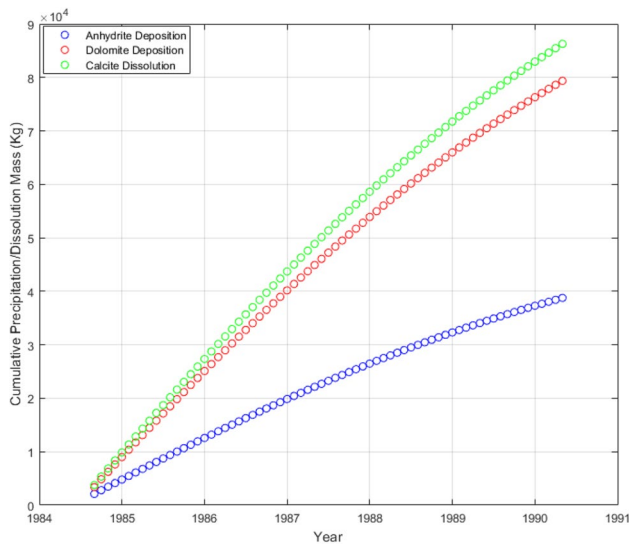


Fig. 21 Amount of rock dissolution and/or scale formation/deposition during seawater injection in the grid block associated with the injection well

Our ad-scale coupled simulator also enabled us to determine the nature of scale deposition and rock dissolution in the grid block associated with the injection well (Fig. 22). Calcium content of the rock is released into seawater (i.e., dissolution of Calcium Carbonate due to presence of incompatible seawater), which increases the porosity. However, other precipitation/deposition processes associated with Anhydrite and Dolomite occurs within the same grid block that reduce the porosity. The interplay between these processes resulted in overall mild decrease of porosity associated with the

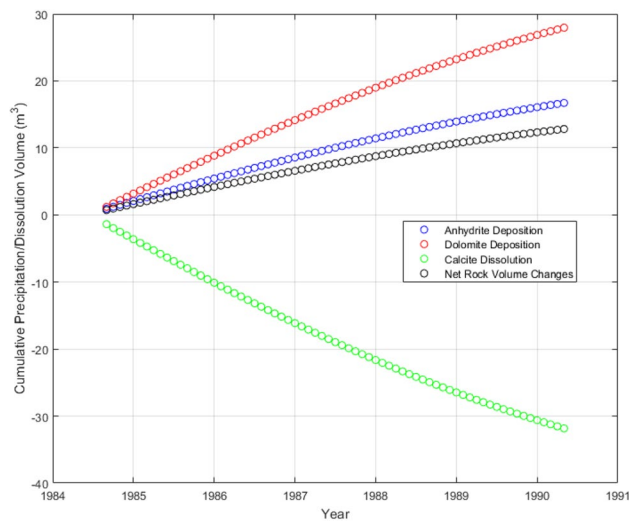


Fig. 22 Volume of rock dissolution and/or scale formation/deposition during seawater injection in the grid block associated with the injection well

injector cell block. The negative values on the cumulative dissolution / precipitation volume axis in Fig. 22 highlights rock dissolution. At a fixed total volume of the grid block, an increase in the grain volume depicted in Fig. 22 demonstrates a reduction in porosity, consistent with the message delivered by Fig. 19.

Another sensitivity analysis was performed to examine if the injected water type would affect the injectivity decline as well as changes in reservoir quality. For this purpose, four different aqueous fluids, with properties detailed in Table 11 were utilized. Besides the formation water and seawater used in earlier realizations, two more brine types, one a low salinity brine and the other a river water associated with a local flowing river, were used. The river water contains the lowest amounts of ions, followed by the low salinity water, among the tested aqueous phases. In Fig. 23, the dimensionless injection flow rate of water is plotted over time for the four simulation cases containing different water phases. These findings can be cross checked against the scale-induced permeability loss in the grid block associated with the injection well (Fig. 24). As expected, injecting formation water into the reservoir can be considered as the comparison baseline since no damage or improvement occurred with respect to the injectivity or near-injector permeability due to perfect compatibility of the injecting and in-situ aqueous phases. Even though the River Water composition is significantly different from that of the Formation Water, its injection into the reservoir does not result in any injectivity loss, and only a very minor impaired permeability is observed at the final year of injection. Due to limited data available for this reservoir except the composition of the aqueous phases, the reason for this observation is unknown. The low salinity water injection resulted in a limited injectivity decline of less than 10%, but about 25% decline in near-wellbore permeability. The worst-case scenario is injecting seawater with

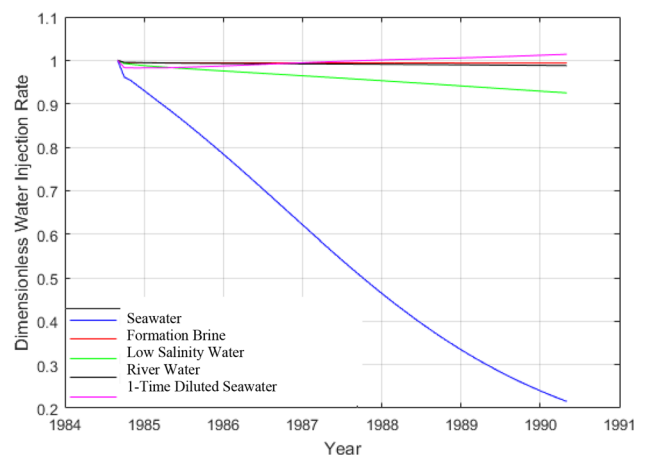
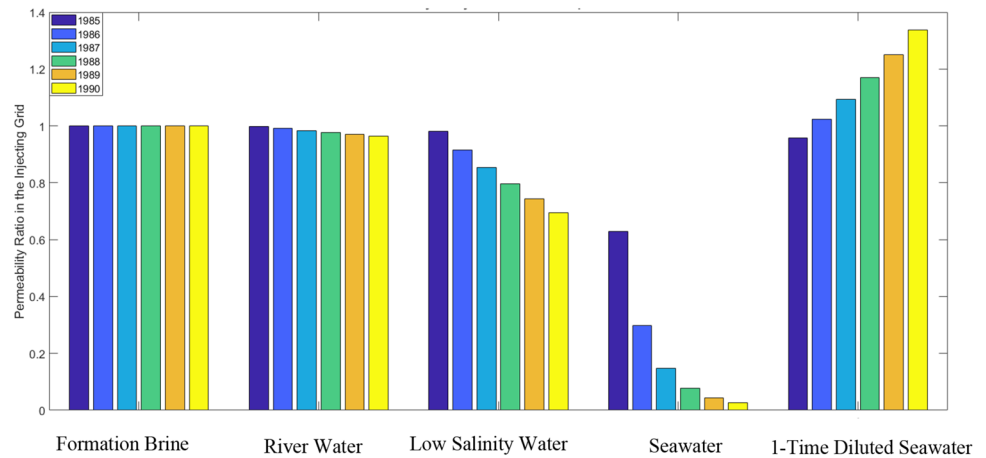


Fig. 23 Dimensionless water injection rate for cases with different aqueous phases

Fig. 24 Permeability alteration profile in the grid block associated with the injection well originated from injecting different aqueous phases



the significant injectivity loss and permeability decline that were discussed earlier. Surprisingly, when the 1-time diluted seawater was injected into the reservoir, it enhanced the injectivity and increased the near wellbore permeability, possibly due to the significant rock dissolution when compared against scale deposition near the injection wellbore.

Conclusions

In this study, a novel reservoir simulator was developed by coupling fluid flow and reactive transport in porous media using MATLAB Reservoir Simulation Toolbox (MRST) and IPHREEQC software packages, respectively. The developed simulator was first validated using experimental data. Once validated, several simulation realizations were conducted to analyze the effect of aqueous phase composition on brine injectivity as well as reservoir quality. The following major conclusions were derived from this study:

- Incompatibility between the formation brine and seawater resulted in major loss in injectivity as well as significant porosity and permeability impairment in the near injector region. The concentration profiles of reacting and non-reacting ions proved that these adverse processes are originated from inorganic scale formation and deposition.
- Rock dissolution and scale formation/deposition are the two processes that control brine injectivity and changes in rock quality. The injecting brine dissolves calcium carbonate, but the free calcium ions in the aqueous phase could react with the sulfate and magnesium ions and form dolomite and anhydrite as inorganic scales as depicted by our simulation results.
- The effect of injecting different aqueous phase types on injectivity and reservoir quality was also determined through a sensitivity analysis. As expected, injecting

compatible aqueous phase (i.e., formation water) with that of in-situ brine into the reservoir does not induce any injectivity loss or reservoir quality impairment. However, changing the injecting brine composition and salinity could result in various degrees of injectivity loss and reservoir quality damage, and could also result in reservoir quality enhancement as depicted in one of our simulation cases. More in-depth analysis of results with detailed rock and fluid information is needed to investigate the balance between the damaging and enhancing mechanisms which could not be fulfilled in this study due to missing several rock and fluid data.

Author contribution The following table contains the authors' contributions to this manuscript, AS, SK, RM, OM: Conceptualization. AS, SK: Methodology. AS, SK, RM, OM: Investigation. AS, RM: Writing—Original Draft. AS, SK, RM, OM: Writing—Review and Editing. SK, RM: Supervision.

Funding This research received no specific grant from any funding agency in the public, commercial, or not-for-profit sectors.

Data availability The authors thank Dr. Moghadasi (Petroleum University of Technology, Iran) for providing data for field-scale simulations. Special thanks to Saeed Parvin (Petroleum University of Technology, Iran) for his supports during this study. For fluid flow modeling, an open-source toolbox known as MATLAB Reservoir Simulation Toolbox (MRST) was used, which is freely available at: <https://www.sintef.no/projectweb/mrst/download/>. For geochemical modeling, PHREEQC Version 3 software was used, which is available through this link: <https://www.usgs.gov/software/phreeqc-version-3>. All the other codes of this study are provided in a public repository at <https://github.com/ahmadrezashojaee/ad-scale>. For running the source codes, first, run the startup.m; then, go to modules/ad-scale/examples and follow the examples on how the model works.

Declarations

Conflict of interest The authors hereby declare that they have no known competing financial interests or personal relationships that could have appeared to influence the work reported in this manuscript.

Open Access This article is licensed under a Creative Commons Attribution 4.0 International License, which permits use, sharing, adaptation, distribution and reproduction in any medium or format, as long as you give appropriate credit to the original author(s) and the source, provide a link to the Creative Commons licence, and indicate if changes were made. The images or other third party material in this article are included in the article's Creative Commons licence, unless indicated otherwise in a credit line to the material. If material is not included in the article's Creative Commons licence and your intended use is not permitted by statutory regulation or exceeds the permitted use, you will need to obtain permission directly from the copyright holder. To view a copy of this licence, visit <http://creativecommons.org/licenses/by/4.0/>.

References

- Abbasi P, Abbasi S, Moghadasi J (2020) Experimental investigation of mixed-salt precipitation during smart water injection in the carbonate formation. *J Mol Liq* 299:112131. <https://doi.org/10.1016/j.molliq.2019.112131>
- Abouie A (2015) Development and application of a compositional wellbore simulator for modeling flow assurance issues and optimization of field production the University of Texas at Austin. <https://repositories.lib.utexas.edu/handle/2152/30286>
- Alpak FO, Lake LW, Embrid SM (1999) Validation of a Modified Carman-Kozeny Equation To Model Two-Phase Relative Permeabilities SPE Annual Technical Conference and Exhibition. <https://doi.org/10.2118/56479-MS>
- AlSofi AM, Wang J, AlBoqmi AM, AlOtaibi MB, Ayirala SC, AlYousef AA (2018) Smartwater synergy with chemical enhanced oil recovery: polymer effects on smartwater. *SPE Reservoir Eval Eng* 22(01):61–77. <https://doi.org/10.2118/184163-PA>
- Amiri M, Moghadasi J, Pordel M (2012) The effect of temperature, pressure, and mixing ratio of the injection water with formation water on strontium sulfate scale formation in the siri oilfield. *Pet Sci Technol* 30(7):635–645. <https://doi.org/10.1080/10916466.2010.489088>
- Bajammal FA, Biyanni HM, Riksa AP, Poitrenaud HM, Mahardhini A (2013) Scale management in mature gas field: case study of peciko international petroleum technology conference. <https://doi.org/10.2523/iptc-16675-ms>
- Bedrikovetsky P, Silva RMP, Daher JS, Gomes JAT, Amorim VC (2009a) Well-data-based prediction of productivity decline due to sulphate scaling. *J Petrol Sci Eng* 68(1):60–70. <https://doi.org/10.1016/j.petrol.2009.06.006>
- Bedrikovetsky PG, Mackay EJ, Silva RMP, Patricio FMR, Rosário FF (2009b) Produced water re-injection with seawater treated by sulphate reduction plant: injectivity decline, analytical model. *J Petrol Sci Eng* 68(1):19–28. <https://doi.org/10.1016/j.petrol.2009.05.015>
- Bedrikovetsky PG, Lopes RP Jr, Gladstone PM, Rosario FF, Bezerra MC, Lima EA (2004) Barium sulphate oilfield scaling: mathematical and laboratory modelling SPE international symposium on oilfield scale. <https://doi.org/10.2118/87457-MS>
- Chandrasekhar S, Sharma H, Mohanty KK (2018) Dependence of wettability on brine composition in high temperature carbonate rocks. *Fuel* 225:573–587. <https://doi.org/10.1016/j.fuel.2018.03.176>
- Charlton SR, Parkhurst DL (2011) Modules based on the geochemical model PHREEQC for use in scripting and programming languages. *Comput Geosci* 37(10):1653–1663. <https://doi.org/10.1016/j.cageo.2011.02.005>
- Chen M, Li X, Tong S, Mohanty K, Wang Y, Yang W, Hazlett R, Lu J (2020) Experimental investigation and numerical modeling of barium sulfate deposition in porous media. *J Petrol Sci Eng* 195:107920. <https://doi.org/10.1016/j.petrol.2020.107920>
- Civan, F (2016) Chapter 4 - Alteration of the Porosity and Permeability of Geologic Formations – Basic and Advanced Relationships. In F. Civan (Ed.), *Reservoir Formation Damage (Third Edition)* (pp. 51-76). Gulf Professional Publishing. <https://doi.org/10.1016/B978-0-12-801898-9.00004-7>
- Dordzie G, Dejam M (2021) Enhanced oil recovery from fractured carbonate reservoirs using nanoparticles with low salinity water and surfactant: a review on experimental and simulation studies. *Adv Coll Interface Sci* 293:102449. <https://doi.org/10.1016/j.cis.2021.102449>
- Fathi SJ, Austad T, Strand S (2012) Water-based enhanced oil recovery EOR by "Smart Water" in carbonate reservoirs SPE EOR conference at oil and gas west Asia. <https://doi.org/10.2118/154570-MS>
- Ghasemian J, Riahi S, Ayatollahi S, Mokhtari R (2019) Effect of salinity and ion type on formation damage due to inorganic scale deposition and introducing optimum salinity. *J Petrol Sci Eng* 177:270–281. <https://doi.org/10.1016/j.petrol.2019.02.019>
- Haghtalab A, Kamali MJ, Shahrabadi A (2014) Prediction mineral scale formation in oil reservoirs during water injection. *Fluid Phase Equilib* 373:43–54. <https://doi.org/10.1016/j.fluid.2014.04.001>
- Haghtalab A, Kamali MJ, Shahrabadi A, Golghanddashti H (2015) Investigation of the precipitation of calcium sulfate in porous media: experimental and mathematical modeling. *Chem Eng Commun* 202(9):1221–1230. <https://doi.org/10.1080/00986445.2014.913583>
- Hajirezaie S, Wu X, Peters CA (2017) Scale formation in porous media and its impact on reservoir performance during water flooding. *J Nat Gas Sci Eng* 39:188–202. <https://doi.org/10.1016/j.jngse.2017.01.019>
- Hajirezaie S, Wu X, Soltanian MR, Sakha S (2019) Numerical simulation of mineral precipitation in hydrocarbon reservoirs and wellbores. *Fuel* 238:462–472. <https://doi.org/10.1016/j.fuel.2018.10.101>
- Hu Y, Mackay E (2018) Reactive transport modelling of a carbonate reservoir under seawater injection. In: SPE international oilfield scale conference and exhibition. <https://doi.org/10.2118/190757-MS>
- Huber C, Shafei B, Parmigiani A (2014) A new pore-scale model for linear and non-linear heterogeneous dissolution and precipitation. *Geochim Cosmochim Acta* 124:109–130. <https://doi.org/10.1016/j.gca.2013.09.003>
- Jordan MM, Collins IR, Mackay EJ (2008) Low sulfate seawater injection for barium sulfate scale control: a life-of-field solution to a complex challenge. *SPE Prod Oper* 23(02):192–209. <https://doi.org/10.2118/98096-PA>
- Kargozarfard Z, Haghtalab A, Ayatollahi S, Badizad MH (2020) Molecular dynamics simulation of calcium sulfate nucleation in homogeneous and heterogeneous crystallization conditions: an application in water flooding. *Ind Eng Chem Res* 59(51):22258–22271. <https://doi.org/10.1021/acs.iecr.0c04290>
- Lie KA (2019) An introduction to reservoir simulation using MATLAB/GNU octave: user guide for the MATLAB reservoir simulation toolbox (MRST). Cambridge University Press. <https://doi.org/10.1017/9781108591416>

- Mackay EJ (2003) Modeling in-situ scale deposition: the impact of reservoir and well geometries and kinetic reaction rates. *SPE Prod Facil* 18(01):45–56. <https://doi.org/10.2118/81830-PA>
- Mackay EJ, Collins IR, Jordan MM, Feasey N (2003a) PWRI: Scale formation risk assessment and management international symposium on oilfield scale. <https://doi.org/10.2118/80385-MS>
- Mackay EJ, Collins IR, Jordan MM, Feasey N (2003b) PWRI: scale formation risk assessment and management international symposium on oilfield scale. <https://doi.org/10.2118/80385-MS>
- Mahani H, Keya AL, Berg S, Nasralla R (2016) Electrokinetics of carbonate/brine interface in low-salinity waterflooding: effect of brine salinity, composition, rock type, and pH on ζ -potential and a surface-complexation model. *SPE J* 22(01):53–68. <https://doi.org/10.2118/181745-PA>
- Mahmoodi A, Nick HM (2022) The interplay between microbial reservoir souring and barite scale formation in hydrocarbon reservoirs. *J Clean Prod* 377:134234. <https://doi.org/10.1016/j.jclepro.2022.134234>
- Masoudi M, Parvin S, Miri R, Kord S, Hellevang H (2020) Implementation of PC-SAFT equation of state into MRST compositional for modelling of asphaltene precipitation. <https://doi.org/10.3997/2214-4609.202011432>
- Merdhah ABM, Yassin AAM, Asli UT (2008) The study of scale formation in oil reservoir during water injection at high - barium and high - salinity formation water. Universiti Teknologi Malaysia. <https://books.google.com/books?id=DiZDAQAACAAJ>
- Moghadasi J, Sharif A, Müller-Steinhagen H, Jamialahmadi M (2006) Prediction of scale formation problems in oil reservoirs and production equipment due to injection of incompatible waters. *Dev Chem Eng Miner Process* 14(3–4):545–566. <https://doi.org/10.1002/apj.5500140319>
- Moghadasi J, Jamialahmadi M, Müller-Steinhagen H, Sharif A (2004) Formation damage due to scale formation in porous media resulting from water injection SPE international symposium and exhibition on formation damage control, Lafayette, Louisiana. <https://doi.org/10.2118/86524-MS>
- Naseri S, Moghadasi J, Jamialahmadi M (2015) Effect of temperature and calcium ion concentration on permeability reduction due to composite barium and calcium sulfate precipitation in porous media. *J Nat Gas Sci Eng* 22:299–312. <https://doi.org/10.1016/j.jngse.2014.12.007>
- Oddo JE, Tomson MB (1994) Why scale forms in the oil field and methods to predict it. *SPE Prod Facil* 9(01):47–54. <https://doi.org/10.2118/21710-pa>
- Olayiwola SO, Dejam M (2020) Effect of silica nanoparticles on the oil recovery during alternating injection with low salinity water and surfactant into carbonate reservoirs SPE annual technical conference and exhibition. <https://doi.org/10.2118/201586-MS>
- Ozen E (2017) Modeling of geochemical reactions with fluid flow simulation for scale precipitation and alkaline/surfactant/polymer flooding processes. <https://repositories.lib.utexas.edu/handle/2152/74900>
- Parkhurst D, Appelo T (1999) User's guide to PHREEQC version 3—a computer program for speciation, batch-reaction, one-dimensional transport, and inverse geochemical calculations (Vol. 99)
- Parvin S, Masoudi M, Sundal A, Miri R (2020) Continuum scale modelling of salt precipitation in the context of CO₂ storage in saline aquifers with MRST compositional. *Int J Greenhouse Gas Control* 99:103075. <https://doi.org/10.1016/j.ijggc.2020.103075>
- Payehghadr M, Eliasi A (2010) Chemical compositions of persian gulf water around the Qeshm island at various seasons. *Asian J Chem* 22:5282–5288
- Rocha AA, Frydman M, da Fontoura SAB, Rosario FF, Bezerra MCM (2001) Numerical modeling of salt precipitation during produced water reinjection international symposium on oilfield scale. <https://doi.org/10.2118/68336-ms>
- Safari H, Jamialahmadi M (2014) Thermodynamics, kinetics, and hydrodynamics of mixed salt precipitation in porous media: model development and parameter estimation. *Transp Porous Media* 101(3):477–505. <https://doi.org/10.1007/s11242-013-0255-6>
- Shabani A, Kalantariasl A, Abbasi S, Shahrabadi A, Aghaei H (2019a) A coupled geochemical and fluid flow model to simulate permeability decline resulting from scale formation in porous media. *Appl Geochem* 107:131–141. <https://doi.org/10.1016/j.apgeochem.2019.06.003>
- Shabani A, Kalantariasl A, Parvazdavani M, Abbasi S (2019b) Geochemical and hydrodynamic modeling of permeability impairment due to composite scale formation in porous media. *J Petrol Sci Eng* 176:1071–1081. <https://doi.org/10.1016/j.petrol.2019.01.088>
- Shirazi M, Kord S, Tamsilian Y (2019) Novel smart water-based titania nanofluid for enhanced oil recovery. *J Mol Liq* 296:112064. <https://doi.org/10.1016/j.molliq.2019.112064>
- Shirdel M (2013) Development of a coupled wellbore-reservoir compositional simulator for damage prediction and remediation. <https://repositories.lib.utexas.edu/handle/2152/21391>
- Shutong P, Sharma M M (1997) A Model for Predicting Injectivity Decline in Water-Injection Wells. *SPE Formation Evaluation*, 12(03):194–201. <https://doi.org/10.2118/28489-PA>
- Sorbie KS, Mackay EJ (2000) Mixing of injected, connate and aquifer brines in waterflooding and its relevance to oilfield scaling. *J Petrol Sci Eng* 27(1):85–106. [https://doi.org/10.1016/S0920-4105\(00\)00050-4](https://doi.org/10.1016/S0920-4105(00)00050-4)
- Todd AC, Yuan MD (1992) Barium and strontium sulfate solid-solution scale formation at elevated temperatures. *SPE Prod Eng* 7(01):85–92. <https://doi.org/10.2118/19762-PA>
- Wu X (2018) Chapter Five-Formation Damage by Inorganic Deposition. In: Yuan B, Wood DA (eds) *Formation damage during improved oil recovery* (pp. 217–242). Gulf Professional Publishing. <https://doi.org/10.1016/B978-0-12-813782-6.00005-1>
- Yuan M, Todd AC, Sorbie KS (1994) Sulphate scale precipitation arising from seawater injection: a prediction study. *Mar Pet Geol* 11(1):24–30. [https://doi.org/10.1016/0264-8172\(94\)90006-X](https://doi.org/10.1016/0264-8172(94)90006-X)
- Zohoorian AH, Moghadasi J, Abbasi S, Jamialahmadi M (2016) Mixed salt scaling in porous media due to water incompatibility: an experimental investigation SPE international oilfield scale conference and exhibition. <https://doi.org/10.2118/179915-MS>

Publisher's Note Springer Nature remains neutral with regard to jurisdictional claims in published maps and institutional affiliations.